

# Bright entanglement and the Einstein–Podolsky–Rosen paradox with coupled parametric oscillators

N. Olivier <sup>a,b</sup>, M.K. Olsen <sup>b,\*</sup>

<sup>a</sup> *École Nationale Supérieure Techniques Avancées, 32 Boulevard Victor, 75739 Paris, France*

<sup>b</sup> *ARC Centre of Excellence for Quantum-Atom Optics, School of Physical Sciences, University of Queensland, Brisbane, Qld 4072, Australia*

Received 17 August 2005; received in revised form 24 September 2005; accepted 27 September 2005

## Abstract

We show that two evanescently coupled  $\chi^{(2)}$  parametric oscillators provide a tunable bright source of quadrature squeezed light, Einstein–Podolsky–Rosen correlations and quantum entanglement. Analysing the system in the above threshold regime, we demonstrate that these properties can be controlled by adjusting the coupling strengths and the cavity detunings. As this can be implemented with integrated optics, it provides a possible route to rugged and stable EPR sources.

© 2005 Elsevier B.V. All rights reserved.

PACS: 42.50.Dv; 42.65.Lm; 03.65.Ud

Keywords: Bright entanglement; Einstein–Podolsky–Rosen paradox; Parametric oscillation

## 1. Introduction

In an earlier publication, Olsen and Drummond [1] showed that two evanescently coupled parametric processes operating below the oscillation threshold inside a pumped Fabry–Perot cavity could be used as a source of spatially separated continuous variable entangled and Einstein–Podolsky–Rosen (EPR) states. Quantum entanglement and the EPR paradox are central to quantum mechanics, with the latter stemming from a famous paper published in 1935 [2], which showed that local realism was not consistent with quantum mechanical completeness. In recent times, there has been increasing attention paid to continuous variable entanglement, often using the optical quadrature amplitudes which are mathematically equivalent to the position and momentum originally considered by EPR [3]. Continuous variable bipartite entanglement can be demonstrated if a set of inequalities developed by Duan et al. [4] are violated. In this work, we extend the

analysis of Olsen and Drummond [1] to the above threshold regime, showing how far above the oscillation threshold these quantum properties are available. In contrast to the below threshold regime where the outputs which exhibit quantum correlations are essentially squeezed vacuum modes, the output beams above threshold can be macroscopically intense.

The first experimental demonstration of the EPR paradox used nondegenerate optical parametric amplification [5], and followed from theoretical work by Reid and Drummond [6–9] which showed that the optical quadrature phase amplitudes have the same mathematical properties as the position and momentum originally used by EPR and, when sufficiently entangled, would allow for an inferred violation of the Heisenberg uncertainty principle. This is completely equivalent to a demonstration of the paradox. Recently, important progress was made toward a demonstration of EPR with bright beams when Villar et al. [10] demonstrated bright entangled outputs from a nondegenerate optical parametric oscillator operating above threshold, although they were not able to make an unambiguous demonstration of the paradox due to losses.

\* Corresponding author. Tel.: +61 7 3346 9826; fax: +61 7 3365 1242.  
E-mail address: [mko@physics.uq.edu.au](mailto:mko@physics.uq.edu.au) (M.K. Olsen).

The scheme we analyse here may provide a more stable route to a demonstration with spatially separated bright beams.

Our system consists of two coupled nonlinear crystals operating inside a pumped Fabry–Perot cavity and is related to a similar scheme using coupled second harmonic generation, first analysed by Bache et al. [11]. The coupling is realised by evanescent overlaps of the intracavity modes inside the nonlinear medium, which can be either a single nonlinear crystal pumped by two spatially separated lasers, or two waveguides with a  $\chi^{(2)}$  component. This type of coupling has already been investigated theoretically and experimentally [12–14]. Peřina et al. [15] introduced the term nonlinear coupler to describe a system of two coupled waveguides without an optical cavity, generically consisting of two parallel optical waveguides coupled by an evanescent overlap of the guided modes. The system without a cavity has been theoretically investigated with both  $\chi^{(3)}$  [16,17], and  $\chi^{(2)}$  nonlinearities. In the latter case, it has been predicted that the light produced in one of the media can be controlled by the light entering the other [18], and that the output beams will show entanglement [19].

Our aim here is to combine and extend these previous analyses and consider two coupled parametric oscillators operating inside a Fabry–Perot cavity in the above threshold regime. A possible advantage of this system is that it is all-integrated, and thus has good robustness and stability, making it a tunable source for bright entangled beams. Moreover, the spatial separation of the output modes means that they do not have to be separated by optical devices before measurements can be made, thus avoiding the losses which would result from this procedure. We note here that this provides an alternative to the previously analysed spatial separation by diffraction within the cavity of the nondegenerate OPO operating above threshold, considered by Lugiato and Castelli [20], Castelli and Lugiato [21], and Zambrini and San Miguel [22]. As the above threshold solutions of our system generally have no simple analytical expressions, most of our results will be presented numerically.

## 2. The system and equations of motion

Remembering the important difference that our scheme operates in the downconversion regime, the overall details are as given by Bache et al. [11]. The optical cavity encloses either two waveguides or one crystal and supports two optical modes at frequencies  $\omega_a, \omega_b$ , where  $2\omega_a \simeq \omega_b$ . We will assume that only the cavity modes at these two frequencies are important. The cavity is pumped at a frequency  $2\omega_L \simeq \omega_b$ , with the two pump beams entering at spatially separated locations. The two inputs may be from separate lasers although it would possibly be better to create them from one laser using beamsplitters. The optical modes inside the nonlinear media are evanescently coupled and we will assume perfect phase matching and equal effective nonlinearities for the two modes.

The effective Hamiltonian for this system can be written as

$$\mathcal{H}_{\text{eff}} = \mathcal{H}_{\text{int}} + \mathcal{H}_{\text{couple}} + \mathcal{H}_{\text{pump}} + \mathcal{H}_{\text{res}}, \quad (1)$$

where  $\mathcal{H}_{\text{int}}$  describes the nonlinear interaction with the  $\chi^{(2)}$  media,  $\mathcal{H}_{\text{couple}}$  the coupling by evanescent waves,  $\mathcal{H}_{\text{pump}}$  the cavity pumping, and  $\mathcal{H}_{\text{res}}$  the cavity damping into zero temperature Markovian reservoirs. The interaction Hamiltonian is

$$\mathcal{H}_{\text{int}} = i\hbar \frac{\kappa}{2} [\hat{a}_1^{\dagger 2} \hat{b}_1 - \hat{a}_1^2 \hat{b}_1^{\dagger} + \hat{a}_2^{\dagger 2} \hat{b}_2 - \hat{a}_2^2 \hat{b}_2^{\dagger}], \quad (2)$$

where  $\hat{a}_k, \hat{b}_k$  are the bosonic annihilation operators for quanta at the frequencies  $\omega_a, \omega_b$  within the crystal  $k$  ( $=1, 2$ ) and  $\kappa$  denotes the effective nonlinearity. The coupling Hamiltonian is

$$\mathcal{H}_{\text{couple}} = \hbar J_a [\hat{a}_1 \hat{a}_2^{\dagger} + \hat{a}_1^{\dagger} \hat{a}_2] + \hbar J_b [\hat{b}_1 \hat{b}_2^{\dagger} + \hat{b}_1^{\dagger} \hat{b}_2], \quad (3)$$

where the  $J_k$  are the coupling parameters at the two frequencies, as described in [11]. The pumping Hamiltonian is

$$\mathcal{H}_{\text{pump}} = i\hbar [\epsilon_1 \hat{b}_1^{\dagger} - \epsilon_1^* \hat{b}_1 + \epsilon_2 \hat{b}_2^{\dagger} - \epsilon_2^* \hat{b}_2], \quad (4)$$

where the  $\epsilon_k$  represent pump fields that will be described classically. Finally, the damping Hamiltonian is

$$\mathcal{H}_{\text{res}} = \hbar \sum_{i=1}^2 (\Gamma_a^k \hat{a}_k^{\dagger} + \Gamma_b^k \hat{b}_k^{\dagger}) + \text{H.c.}, \quad (5)$$

where the  $\Gamma^k$  represent bath operators at the two frequencies.

Following the usual methods [23,24], the system Hamiltonian is mapped onto a Fokker–Planck equation in the positive-P representation [25–27] which has a positive-definite diffusion matrix and thus may be mapped onto stochastic differential equations. Making the correspondence between the set of operators ( $\hat{a}_j, \hat{a}_j^{\dagger}, \hat{b}_j, \hat{b}_j^{\dagger}$ ) ( $j = 1, 2$ ) and the set of c-number variables ( $\alpha_j, \alpha_j^+, \beta_j, \beta_j^+$ ), we find the following set of equations:

$$\begin{aligned} \frac{d\alpha_1}{dt} &= -(\gamma_a + i\Delta_a)\alpha_1 + \kappa\alpha_1^+\beta_1 + iJ_a\alpha_2 + \sqrt{\kappa\beta_1}\eta_1(t), \\ \frac{d\alpha_1^+}{dt} &= -(\gamma_a - i\Delta_a)\alpha_1^+ + \kappa\alpha_1\beta_1^+ - iJ_a\alpha_2^+ + \sqrt{\kappa\beta_1^+}\eta_2(t), \\ \frac{d\alpha_2}{dt} &= -(\gamma_a + i\Delta_a)\alpha_2 + \kappa\alpha_2^+\beta_2 + iJ_a\alpha_1 + \sqrt{\kappa\beta_2}\eta_3(t), \\ \frac{d\alpha_2^+}{dt} &= -(\gamma_a - i\Delta_a)\alpha_2^+ + \kappa\alpha_2\beta_2^+ - iJ_a\alpha_1^+ + \sqrt{\kappa\beta_2^+}\eta_4(t), \\ \frac{d\beta_1}{dt} &= \epsilon_1 - (\gamma_b + i\Delta_b)\beta_1 - \frac{\kappa}{2}\alpha_1^2 + iJ_b\beta_2, \\ \frac{d\beta_1^+}{dt} &= \epsilon_1^* - (\gamma_b - i\Delta_b)\beta_1^+ - \frac{\kappa}{2}\alpha_1^{+2} - iJ_b\beta_2^+, \\ \frac{d\beta_2}{dt} &= \epsilon_2 - (\gamma_b + i\Delta_b)\beta_2 - \frac{\kappa}{2}\alpha_2^2 + iJ_b\beta_1, \\ \frac{d\beta_2^+}{dt} &= \epsilon_2^* - (\gamma_b - i\Delta_b)\beta_2^+ - \frac{\kappa}{2}\alpha_2^{+2} - iJ_b\beta_1^+, \end{aligned} \quad (6)$$

where  $\Delta_{a,b}$  represents a cavity detuning from the two resonances, so that for a pump laser at angular frequency  $2\omega_L$ ,

one has  $\Delta_a = \omega_a - \omega_L$  and  $\Delta_b = \omega_b - 2\omega_L$ . The real Gaussian noise terms have the correlations  $\eta_j(t) = 0$  and  $\eta_j(t)\eta_k(t') = \delta_{jk}\delta(t-t')$ . Note that, due to the independence of the noise sources,  $\alpha_k$  ( $\beta_k$ ) and  $\alpha_k^+$  ( $\beta_k^+$ ) are not complex conjugate pairs, except in the mean over a large number of stochastic integrations. However, these equations do allow us to calculate the expectation values of any desired time-normally ordered operator moments, exactly as required to calculate spectral correlations.

### 3. Linearised analysis

Although Eq. (6) can be integrated numerically, we find that, as long as we are not concerned with the operating regime in the immediate vicinity of the oscillation threshold,

$$A_0 = \frac{\sqrt{2}}{\kappa} \sqrt{(J_a - \Delta_a)(J_b - \Delta_b) - \gamma_a \gamma_b + \sqrt{\kappa^2 \epsilon^2 - ((J_a - \Delta_a)\gamma_b + (J_b - \Delta_b)\gamma_a)^2}}. \quad (11)$$

we may linearise the equations around their classical steady-state solutions. This allows for a simple way of calculating the spectral correlations [23,28], by treating the system as a Ornstein–Uhlenbeck process [29]. The region close to threshold would require a full numerical stochastic treatment but is not usually considered experimentally due to the high degree of stability which lasers would need to operate there.

#### 3.1. Steady-state equations

We begin by dividing the variables into a steady-state mean value and a fluctuation part, e.g.,  $\alpha_i \rightarrow \alpha_i^{ss} + \delta\alpha_i$ . In order to simplify our results, we will make the following assumptions:

- The pumping terms for both crystals are real and equal  $\epsilon_1 = \epsilon_2 = \epsilon$ .
- Given this assumption, and with the detunings, loss rates and nonlinearities of the two subsystems equal, we may proceed as with the below threshold results [1], and set  $\beta_1^{ss} = \beta_2^{ss} = \beta^{ss}$ . In general this will not be the case.

We then find a new set of equations for the steady-state solutions:

$$\begin{cases} \alpha_1^{ss}(\gamma_a + i\Delta_a) = \kappa\alpha_1^{ss*}\beta^{ss} + iJ_a\alpha_2^{ss}, \\ \alpha_2^{ss}(\gamma_a + i\Delta_a) = \kappa\alpha_2^{ss*}\beta^{ss} + iJ_a\alpha_1^{ss}, \\ \frac{\kappa}{2}\alpha_1^{ss2} = \epsilon - (\gamma_b + i\Delta_b - iJ_b)\beta^{ss}, \\ \frac{\kappa}{2}\alpha_2^{ss2} = \epsilon - (\gamma_b + i\Delta_b - iJ_b)\beta^{ss}. \end{cases} \quad (7)$$

The last two of the equations above imply that

$$(\alpha_1^{ss})^2 = (\alpha_2^{ss})^2 = (\alpha^{ss})^2, \quad (8)$$

suggesting that  $\alpha_1^{ss} = \pm\alpha_2^{ss}$ . We find that the stable solution is that with  $\alpha_2^{ss} = \alpha_1^{ss}$ , which leads to

$$\begin{cases} \alpha^{ss}(\gamma_a + i\Delta_a - iJ_a) = \kappa\alpha^{ss*}\beta^{ss}, \\ \frac{\kappa}{2}\alpha^{ss2} = \epsilon - (\gamma_b + i\Delta_b - iJ_b)\beta^{ss}. \end{cases} \quad (9)$$

These equations may be solved to give

$$\beta_i^{ss} = \frac{\gamma_a - i(J_a - \Delta_a)}{\kappa} \times e^{2i\text{Arccos}\left(\sqrt{\frac{1}{2} + \frac{1}{2\kappa\epsilon}\sqrt{\epsilon^2\kappa^2 - ((J_a - \Delta_a)\gamma_b + (J_b - \Delta_b)\gamma_a)^2}}\right)}, \quad (10)$$

$$\alpha_i^{ss} = \pm A_0 e^{i\text{Arccos}\left(\sqrt{\frac{1}{2} + \frac{1}{2\kappa\epsilon}\sqrt{\epsilon^2\kappa^2 - ((J_a - \Delta_a)\gamma_b + (J_b - \Delta_b)\gamma_a)^2}}\right)},$$

where

In the case where  $\Delta_a = J_a$ ,  $\Delta_b = J_b$ , we find the same solutions as for the uncoupled optical parametric oscillator (OPO) above threshold,

$$\begin{cases} \beta^{ss} = \frac{\gamma_a}{\kappa}, \\ \alpha^{ss} = \pm\sqrt{\frac{2}{\kappa}\left(\epsilon - \frac{\gamma_a\gamma_b}{\kappa}\right)}. \end{cases} \quad (12)$$

#### 3.2. The drift matrix

We can now write the equation for the fluctuation vector,

$$\delta\tilde{x} = [\delta\alpha_1, \delta\alpha_1^+, \delta\alpha_2, \delta\alpha_2^+, \delta\beta_1, \delta\beta_1^+, \delta\beta_2, \delta\beta_2^+]^T, \quad (13)$$

to first-order in these fluctuations, as

$$d\delta\tilde{x} = A\delta\tilde{x}dt + B dW, \quad (14)$$

where

$$A = \begin{bmatrix} A_{aa} & A_{ab} \\ -A_{ab}^* & A_{bb} \end{bmatrix} \quad (15)$$

and

$$B = \begin{bmatrix} B_{aa} & 0 \\ 0 & 0 \end{bmatrix}, \quad (16)$$

with

$$B_{aa} = \begin{bmatrix} \sqrt{\kappa\beta^{ss}} & 0 & 0 & 0 \\ 0 & \sqrt{\kappa\beta^{ss*}} & 0 & 0 \\ 0 & 0 & \sqrt{\kappa\beta^{ss}} & 0 \\ 0 & 0 & 0 & \sqrt{\kappa\beta^{ss*}} \end{bmatrix} \quad (17)$$

and

$$A_{aa} = \begin{bmatrix} -(\gamma_a + iJ_a) & \kappa\beta^{ss} & iJ_a & 0 \\ \kappa\beta^{ss*} & -(\gamma_a - iJ_a) & 0 & -iJ_a \\ +iJ_a & 0 & -(\gamma_a + iJ_a) & \kappa\beta^{ss} \\ 0 & -iJ_a & \kappa\beta^{ss*} & -(\gamma_a - iJ_a) \end{bmatrix} \quad (18)$$

and

$$A_{ab} = \begin{bmatrix} \kappa\alpha^{ss*} & 0 & 0 & 0 \\ 0 & \kappa\alpha^{ss} & 0 & 0 \\ 0 & 0 & \kappa\alpha^{ss*} & 0 \\ 0 & 0 & 0 & \kappa\alpha^{ss} \end{bmatrix} \quad (19)$$

and

$$A_{bb} = \begin{bmatrix} -(\gamma_b + iJ_b) & 0 & iJ_b & 0 \\ 0 & -(\gamma_b - iJ_b) & 0 & -iJ_b \\ iJ_b & 0 & -(\gamma_b + iJ_b) & 0 \\ 0 & -iJ_b & 0 & -(\gamma_b - iJ_b) \end{bmatrix}. \quad (20)$$

In Eq. (14),  $dW$  is a vector of real Wiener increments. The essential condition for this expansion to be valid is that the fluctuations stay small. The area of validity is easily found by examination of the eigenvalues of the fluctuation drift matrix for the system. The fluctuations will not tend to grow as long as none of the eigenvalues of the matrix  $A$  develop a positive real part, at which point the linearised fluctuation analysis is no longer valid, as the fluctuations can then grow exponentially. As in the below-threshold analysis of [1], we define  $\epsilon_c$  the value of the pump at which the threshold is reached,

$$\epsilon_c = \sqrt{[\gamma_a^2 + (J_a - \Delta_a)^2][\gamma_b^2 + (J_b - \Delta_b)^2]}/\kappa. \quad (21)$$

We found that the solutions we use are stable everywhere but at threshold by numerical examination of the maximum values of the real parts of the eigenvalues of the  $A$  matrix. For the parameter values  $\Delta_a = J_a$  and  $\Delta_b = J_b$ , for which we find the best spectral results, the stability diagram is the same as in the uncoupled case, with the stable below threshold solutions being

$$\alpha_j^{ss} = 0, \quad \beta_j^{ss} = \epsilon/\gamma_b, \quad (22)$$

while the stable above threshold solutions are as given in Eq. (12). In the general case, with different pump values and detunings different from the couplings, it is only possible to calculate the stability numerically and the diagram becomes more complicated as it depends on a larger number of parameters.

#### 4. Spectral correlations

In order to calculate the phase-dependent spectral correlations necessary to demonstrate entanglement and the EPR paradox, we begin by defining the quadrature amplitudes as

$$\hat{X}_j^\theta = \hat{a}_j e^{-i\theta} + \hat{a}_j^\dagger e^{i\theta}, \quad (23)$$

with

$$\hat{X}_j^O = \hat{X}_j, \quad \hat{X}_j^\pi = \hat{Y}_j. \quad (24)$$

We may calculate any desired time normally ordered spectral correlations inside the cavity using the simple formula [29],

$$S(\omega) = (A + i\omega\mathbf{1})^{-1} B B^T (A^T - i\omega\mathbf{1})^{-1}, \quad (25)$$

with the variances of interest inside and outside the cavity being related by [23]

$$S^{\text{out}}(\omega) = 1 + 2\gamma_a S(\omega). \quad (26)$$

#### 4.1. Entanglement and the EPR paradox

The entanglement criterion we will use has been outlined by Dechoum et al. [30], following from criteria developed by Duan et al. [4] which are based on the inseparability of the total density matrix and are necessary and sufficient for Gaussian states. To demonstrate entanglement between the modes, we will define the combined quadratures

$$\begin{aligned} \hat{X}_\pm^\theta &= \hat{X}_1^\theta \pm \hat{X}_2^\theta, \\ \hat{Y}_\pm^\theta &= \hat{Y}_1^\theta \pm \hat{Y}_2^\theta, \end{aligned} \quad (27)$$

where  $\hat{Y}^\theta = \hat{X}^{\theta+\pi/2}$ . Following the treatment of [30], entanglement is guaranteed provided that

$$S_{X_\pm^\theta}^{\text{out}} + S_{Y_\mp^\theta}^{\text{out}} < 4. \quad (28)$$

To examine the utility of the system for the production of states which exhibit the EPR paradox, we follow the approach of Reid [7]. We assume that a measurement of the  $\hat{X}_1$  quadrature, for example, will allow us to infer, with some error, the value of the  $\hat{X}_2$  quadrature, and similarly for the  $\hat{Y}_j$  quadratures. This allows us to make linear estimates of the quadrature variances, which are then minimised to give the inferred output variances,

$$\begin{aligned} S_{\text{inf}}^{\text{out}}(\hat{X}_1) &= S_{X_1}^{\text{out}} - \frac{[V(\hat{X}_1, \hat{X}_2)]^2}{S_{X_2}^{\text{out}}}, \\ S_{\text{inf}}^{\text{out}}(\hat{Y}_1) &= S_{Y_1}^{\text{out}} - \frac{[V(\hat{Y}_1, \hat{Y}_2)]^2}{S_{Y_2}^{\text{out}}}, \end{aligned} \quad (29)$$

where  $V(A, B) = \langle AB \rangle - \langle A \rangle \langle B \rangle$  should be considered as an output spectral covariance. The inferred variances for the  $\hat{X}_2$  and  $\hat{Y}_2$  quadratures are simply found by swapping the indices 1 and 2. As the  $\hat{X}_j$  and  $\hat{Y}_j$  operators do not commute, the products of the actual variances obey a Heisenberg uncertainty relation, which means we find a demonstration of the EPR paradox whenever

$$S_{\text{inf}}^{\text{out}}(\hat{X}_j) S_{\text{inf}}^{\text{out}}(\hat{Y}_j) \leq 1. \quad (30)$$

### 5. Resonant cavity

With the cavity at resonance for all modes in the above threshold regime, the expressions for the spectral variances become extremely complicated. The evanescent coupling means that the intracavity fields are now complex, so that the optimum correlations will not be found in the  $X_j$  and  $Y_j$  quadratures as in the normal OPO, but at some other phase angle, as found previously for second harmonic generation in detuned cavities [31]. Experimentally, this does not present a problem as the local oscillator phase is normally swept across all angles, which must include the optimum angle. We find that changing  $J_b$  mainly serves to change the angle of maximum squeezing. Changing  $J_a$  changes both the frequency at which the maximum of squeezing is found, and the maximum value. We find that this device is not as efficient at producing squeezed single-mode outputs as the normal OPO, but as we are interested in the quantum correlations between the output modes, this is not a problem.

Numerical calculations of the entanglement criteria for different values of  $J_a$  and optimised phase angles show that when operating above threshold with both cavities resonant, the degree of entanglement increases as  $J_a$  is increased but the maximum value is found at an increasing value of the frequency. On the other hand, changing  $J_b$  has an influence on the maximum value when  $J_a$  is small, but mainly changes the best angle for bigger values of  $J_a$ . We find that a reasonable degree of entanglement is present only at several cavity linewidths away from zero frequency, where the light will not be of a high intensity. An investigation of the EPR correlations at resonance shows only small inferred violations of the Heisenberg uncertainty principle, also evident at several linewidths from zero frequency. As with the entanglement criteria, changing  $J_b$  serves to change the angle of the maximum violation, without changing its degree of violation, while changing  $J_a$  changes both the degree and the frequency of the maximum violation. As expected, these results are symmetric for both outputs of the device. As our objective is to propose and analyse the device as a bright source of quantum entanglement, we will not present resonant results here, but will show in the next section how cavity detunings can be used to optimise the performance.

### 6. Optimisation via detuning

Although optical systems usually exhibit their best performance when the cavity is resonant for the different modes involved in the interactions, we find here that detuning the cavity by the appropriate amount for the two frequencies improves the quantum correlations which we are investigating and also allows for some simplification of the theoretical analysis. With the detuning such that  $\Delta_a = J_a$  and  $\Delta_b = J_b$ , the steady-state solutions for the individual modes are as given in Eq. (12). By analogy with many coupled two-mode systems, we define the sum and difference modes,  $A_p = \alpha_1 + \alpha_2$  and  $A_m = \alpha_1 - \alpha_2$ , and sim-

ilarly for  $B_p$  and  $B_m$ . We have already found the mean-field solutions for these as

$$\begin{aligned} A_p^{ss} &= \alpha_1^{ss} + \alpha_2^{ss} = \pm 2\sqrt{2\left(\epsilon - \frac{\gamma_a\gamma_b}{\kappa}\right)}/\kappa, \\ A_m^{ss} &= \alpha_1^{ss} - \alpha_2^{ss} = 0, \\ B_p^{ss} &= \beta_1^{ss} + \beta_2^{ss} = 2\beta_{ss} = 2\gamma_a/\kappa, \\ B_m^{ss} &= \beta_1^{ss} - \beta_2^{ss} = 0, \end{aligned} \tag{31}$$

so that we may write the equations of motion for their linearised fluctuations (dropping the ss superscripts for notational simplicity) as

$$\begin{aligned} \frac{d}{dt}\delta A_p &= -\gamma_a\delta A_p + \frac{\kappa}{2}\left(A_p^+\delta B_p + B_p\delta A_p^+\right) + \sqrt{\kappa B_p/2}(\eta_1 + \eta_3), \\ \frac{d}{dt}\delta A_p^+ &= -\gamma_a\delta A_p^+ + \frac{\kappa}{2}\left(A_p\delta B_p^+ + B_p^+\delta A_p\right) + \sqrt{\kappa B_p^+/2}(\eta_2 + \eta_4), \\ \frac{d}{dt}\delta A_m &= -(\gamma_a + 2iJ_a)\delta A_m + \frac{\kappa}{2}\left(A_m^+\delta B_p + B_p\delta A_m^+\right) \\ &\quad + \sqrt{\kappa B_p/2}(\eta_1 - \eta_3), \\ \frac{d}{dt}\delta A_m^+ &= -(\gamma_a - 2iJ_a)\delta A_m^+ + \frac{\kappa}{2}\left(A_m\delta B_p^+ + B_p^+\delta A_m\right) \\ &\quad + \sqrt{\kappa B_p^+/2}(\eta_2 - \eta_4), \\ \frac{d}{dt}\delta B_p &= -\gamma_b\delta B_p - \frac{\kappa}{2}A_p\delta A_p, \\ \frac{d}{dt}\delta B_p^+ &= -\gamma_b\delta B_p^+ - \frac{\kappa}{2}A_p^+\delta A_p^+, \\ \frac{d}{dt}\delta B_m &= -(\gamma_b + 2iJ_b)\delta B_m - \frac{\kappa}{2}A_p\delta A_m, \\ \frac{d}{dt}\delta B_m^+ &= -(\gamma_b - 2iJ_b)\delta B_m^+ - \frac{\kappa}{2}A_p^+\delta A_m^+. \end{aligned} \tag{32}$$

The  $\eta_j$  have the same properties as those used in Eq. (6). With the detunings set equal to the evanescent couplings, we now find that the interesting correlations are optimised at the quadrature angles  $\theta = 0, \pi/2$ , so that we may define

$$\begin{aligned} X_p &= A_p + A_p^+ = X_1 + X_2, \\ X_m &= A_m + A_m^+ = X_1 - X_2, \\ Y_p &= -i(A_p - A_p^+) = Y_1 + Y_2, \\ Y_m &= -i(A_m - A_m^+) = Y_1 - Y_2. \end{aligned} \tag{33}$$

We can now give simple analytical expressions for the output spectra of these combined quadratures, finding

$$\begin{aligned} S_{X_p}^{\text{out}}(\omega) &= 2 + \frac{4\gamma_a^2(\gamma_b^2 + \omega^2)}{\gamma_b^2\omega^2 + (\kappa^2\alpha^2 + \omega^2)^2}, \\ S_{X_m}^{\text{out}}(\omega) &= 2 + \frac{4\gamma_a^2[\omega^2 + 4(\gamma_a^2 - J_a^2)]}{4\gamma_a^2\omega^2 + (\omega^2 - 4J_a^2)^2}, \\ S_{Y_p}^{\text{out}}(\omega) &= 2 - \frac{4\gamma_a^2(\gamma_b^2 + \omega^2)}{(\kappa^2\alpha^2 + \omega^2)^2 + 4\gamma_a^2(\gamma_b^2 + \omega^2) - 4\gamma_a\gamma_b\kappa^2\alpha^2}, \\ S_{Y_m}^{\text{out}}(\omega) &= 2 + \frac{4\gamma_a^2(4J_a^2 - \omega^2)}{4\gamma_a^2\omega^2 + (4J_a^2 - \omega^2)^2}. \end{aligned} \tag{34}$$

where  $\alpha = \sqrt{2(\epsilon - \epsilon_c)}/\kappa$ .

The results for  $S_{X_m}^{\text{out}}(\omega)$ ,  $S_{Y_p}^{\text{out}}(\omega)$  and  $S_{Y_m}^{\text{out}}(\omega)$  are presented graphically in Fig. 1, for different ratios  $\epsilon/\epsilon_c$ . We can see that the best squeezing quadrature is  $Y_p$  which still exhibits  $\approx 50\%$  squeezing well above the oscillation threshold. The quadratures  $X_m$  and  $Y_m$  show only a very small degree of squeezing, while  $X_p$  is antisqueezed at all frequencies. We note that the degree of squeezing we observe in  $Y_p$  with this detuning is more than was available without detuning.

The solutions given in Eq. (34) are sufficient for us to investigate the degree of entanglement and the EPR correlations, although the expressions obtained by combining these in the appropriate manners are very complex. We will, therefore, present the results graphically. In Fig. 2, we show how the entanglement correlation for  $Y_p$  and  $X_m$  changes as the ratio  $\epsilon/\epsilon_c$  increases. We can see that

the maximum violation becomes less as the pumping is increased, and also moves away from zero frequency. Increasing the pump both deteriorates the maximum value and shifts it to higher frequencies. Unlike the cases where  $J_i \neq \Delta_i$ , the pump amplitude does not depend on the couplings or detunings, and is therefore lower for the same ratio of critical pump amplitude than in these cases.

As shown in Fig. 3, increasing  $J_a$  gives better entanglement, and also shifts the maximum values to just over zero frequency. The maximum degree of entanglement which we observe is once again better with the detuning. In Fig. 4, we present the results for the EPR correlations, with  $J_b$  held constant at a value of  $\gamma_b$  while  $J_a$  is increased. Changing  $J_a$  changes both the amount and the frequency of the maximum violation, with this bifurcating as  $J_a$

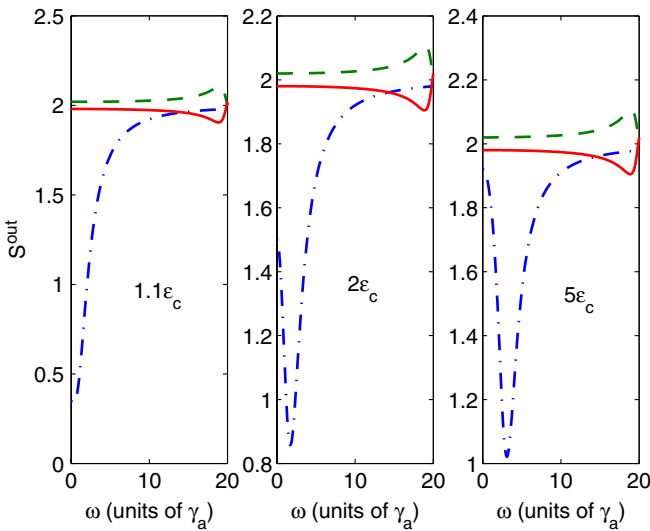


Fig. 1.  $S^{\text{out}}$  with  $\gamma_a = \gamma_b = J_b = \Delta_b = 1$ ,  $J_a = \Delta_a = 10$ . The full lines are for  $X_m$ , the dashed lines are for  $Y_m$  and the dashed-dotted lines are for  $Y_p$ . Note that the vertical axes are not aligned and that a value below 2 represents squeezing.

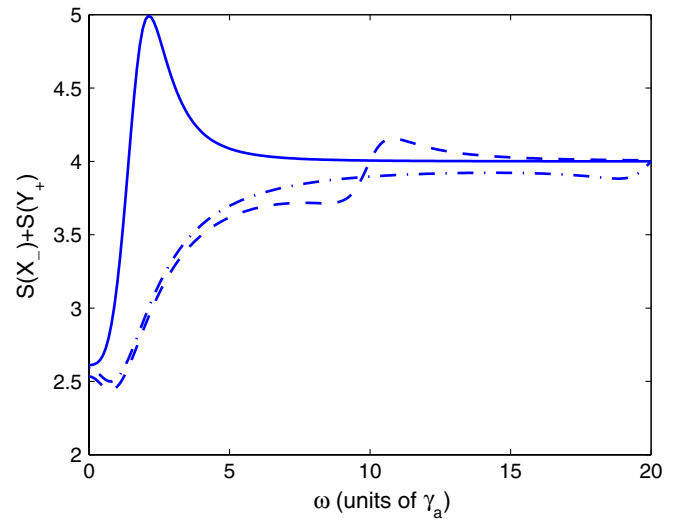


Fig. 3.  $S_{X_m}^{\text{out}} + S_{Y_p}^{\text{out}}$  with  $\gamma_a = \gamma_b = J_b = \Delta_b = 1$ ,  $J_a = \Delta_a$  and  $\epsilon = 1.2\epsilon_c$ . The full line is for  $J_a = 1$ , the dashed line is for  $J_a = 5$  and the dash-dotted line is for  $J_a = 10$ .

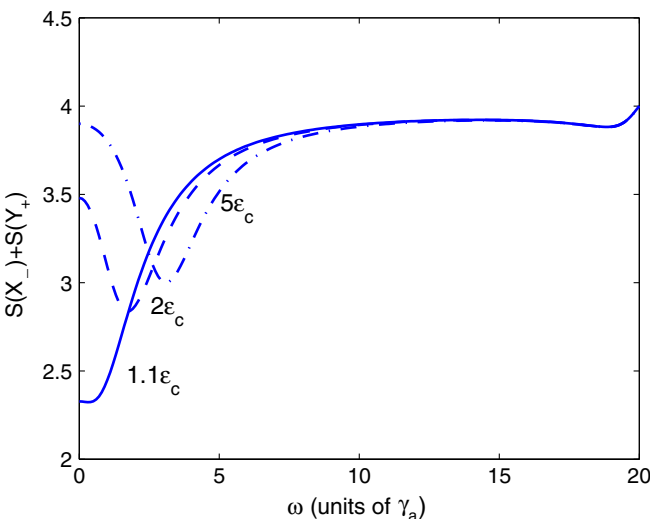


Fig. 2.  $S_{X_m}^{\text{out}} + S_{Y_p}^{\text{out}}$  with  $\gamma_a = \gamma_b = J_b = \Delta_b = 1$ ,  $J_a = \Delta_a = 10$ , and different pump values. A value of less than 4 represents bipartite entanglement.

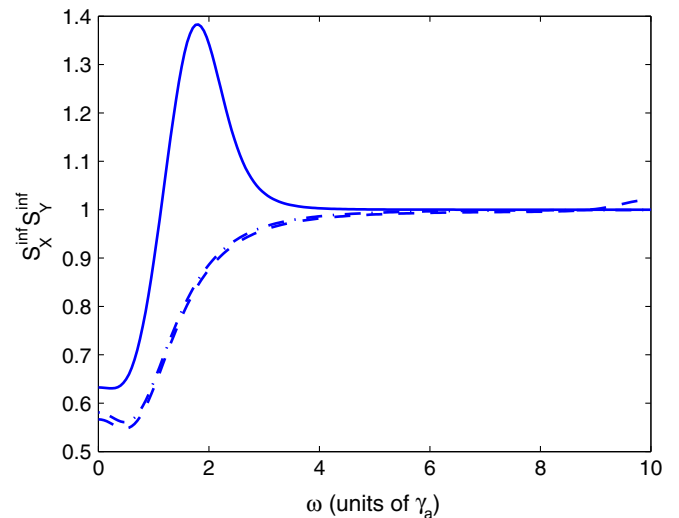


Fig. 4. Demonstration of the EPR correlation for  $J_b = \gamma_a = \gamma_b = \Delta_b = 1$  and  $J_a = \Delta_a = 1$  (solid line), 5 (dashed line), and 10 (dash-dotted line). The pump amplitude is  $\epsilon = 1.1\epsilon_c$ .

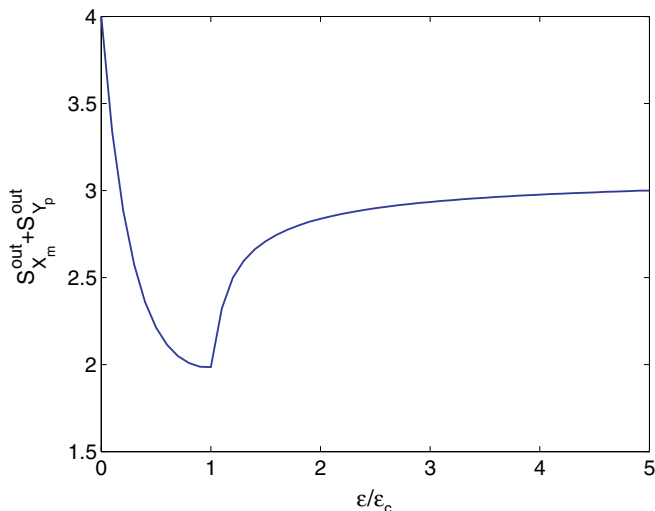


Fig. 5. Maximum entanglement as a function of the pumping, with  $\gamma_a = \gamma_b = J_b = \Delta_b = 1$ , and  $J_a = \Delta_a = 10$ .

increases. This correlation is much less sensitive to changes in  $J_b$ , which only have a small influence. As expected, these results are the same for both outputs of the device. Compared with the resonant case, the EPR correlations of the detuned system show a much larger maximum inferred violation of the Heisenberg inequality and the spectra are less bifurcated.

### 6.1. Evolution of correlations as a function of pumping

In this section, we examine how the correlations evolve as the pumping is increased from zero to above the threshold value, with the caveat that our linearised results in the immediate neighbourhood of the threshold are of limited validity. In Fig. 5, we have plotted the maximum entanglement found between the  $Y_p$  and  $X_m$  quadratures as a func-

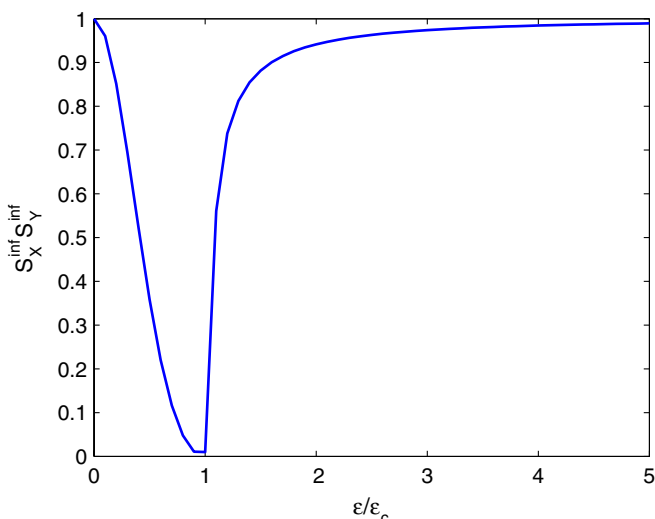


Fig. 6. Maximum demonstration of the EPR paradox as a function of the pumping, with  $\gamma_a = \gamma_b = J_b = \Delta_b = 1$ , and  $J_a = \Delta_a = 10$ .

tion of the pumping. Noting that the output beams become more intense as the pumping increases, we see that a good degree of bright entanglement should be available from this system. From Fig. 6, where the minimum value of the product of the inferred variances is plotted, we see that the demonstration of the EPR paradox is not as robust above threshold as the entanglement. In fact it has almost disappeared at  $\epsilon = 1.5\epsilon_c$ .

## 7. Conclusion

This system exhibits a wide range of behaviors and is potentially an easily tunable source of entanglement and states which exhibit the EPR paradox. In the above threshold regime which we have analysed here, it can be used to produce bright entangled beams. The entangled beams produced can be degenerate in both frequency and polarisation, unlike those of the nondegenerate OPO, and would exit the cavity at spatially separated locations. The spatial separation of the output modes means that they do not have to be separated by optical devices before measurements can be made, saving the unavoidable losses which would result from this procedure. This may be a real operational advantage over the nondegenerate OPO, which is also known to produce nonclassical states. The tunability that exists because of the number of different parameters which can be experimentally accessed, such as the coupling strength, the pump intensities and the detunings, may make it interesting for a range of potential applications which would require the availability of states of the electromagnetic field with varying degrees of nonclassicality. Since this type of system is compatible with integrated optics techniques, it may provide a more robust source of bright entangled beams than interferometers that use discrete optical components.

## Acknowledgements

This research was partially supported by the Australian Research Council. Nicolas Olivier thanks the ARC Centre of Excellence for Quantum-Atom Optics and the University of Queensland for generous hospitality.

## References

- [1] M.K. Olsen, P.D. Drummond, Phys. Rev. A 71 (2005) 53803.
- [2] A. Einstein, B. Podolsky, N. Rosen, Phys. Rev. 47 (1935) 777.
- [3] S.L. Braunstein, A.K. Pati (Eds.), Quantum Information with Continuous Variables, Kluwer Academic, Dordrecht, 2003.
- [4] L.-M. Duan, G. Giedke, J.I. Cirac, P. Zoller, Phys. Rev. Lett. 84 (2000) 2722.
- [5] Z.Y. Ou, S.F. Pereira, H.J. Kimble, K.C. Peng, Phys. Rev. Lett. 68 (1992) 3663.
- [6] M.D. Reid, P.D. Drummond, Phys. Rev. Lett. 60 (1988) 2731.
- [7] M.D. Reid, Phys. Rev. A 40 (1989) 913.
- [8] M.D. Reid, P.D. Drummond, Phys. Rev. A 40 (1989) 4493.
- [9] P.D. Drummond, M.D. Reid, Phys. Rev. A 41 (1990) 3930.
- [10] A.S. Villar, L.S. Cruz, K.N. Cassemiro, M. Martinelli and P. Nussenzveig, quant-ph/0506139.

- [11] M. Bache, Yu.B. Gaididei, P.L. Christiansen, *Phys. Rev. A* 67 (2003) 043802.
- [12] L. Fabiny, P. Colet, R. Roy, D. Lenstra, *Phys. Rev. A* 47 (1993) 4287.
- [13] M. Silber, L. Fabiny, K. Wiesenfeld, *J. Opt. Soc. Am. B* 10 (1993) 1121.
- [14] Y. Braiman, T.A.B. Kennedy, K. Wiesenfeld, A. Khibnik, *Phys. Rev. A* 52 (1995) 1500.
- [15] J. Peřina Jr., J. Peřina, in: E. Wolf (Ed.), *Progress in Optics*, Elsevier, Amsterdam, 2000.
- [16] A.-B.M.A. Ibrahim, B.A. Umarov, M.R.B. Wahiddin, *Phys. Rev. A* 61 (2000) 043804.
- [17] S.A. Podoshvedov, J. Noh, K. Kim, *Opt. Commun.* 212 (2002) 115.
- [18] L. Miřta Jr., J. Herec, V. Jelínek, J. Řeháček, J. Peřina, *J. Opt. B* 2 (2000) 726.
- [19] J. Herec, J. Fiurářek, L. Miřta Jr., *J. Opt. B* 5 (2003) 419.
- [20] L.A. Lugiato, F. Castelli, *Phys. Rev. Lett.* 68 (1992) 3284.
- [21] F. Castelli, L.A. Lugiato, *J. Mod. Opt.* 44 (1997) 765.
- [22] R. Zambrini, M. San Miguel, *Phys. Rev. A* 66 (2002) 023807.
- [23] D.F. Walls, G.J. Milburn, *Quantum Optics*, Springer-Verlag, Berlin, 1995.
- [24] C.W. Gardiner, P. Zoller, *Quantum Noise*, Springer-Verlag, Berlin, 2000.
- [25] P.D. Drummond, C.W. Gardiner, *J. Phys. A* 13 (1980) 2353.
- [26] H.-Y. Fan, M. Xiao, *Phys. Lett. A* 224 (1998) 256.
- [27] L.I. Plimak, M. Fleischhauer, M.K. Olsen, M.J. Collett, *Phys. Rev. A* 67 (2003) 013812.
- [28] C.W. Gardiner, M.J. Collett, *Phys. Rev. A* 31 (1985) 3761.
- [29] C.W. Gardiner, *Handbook of Stochastic Methods*, Springer-Verlag, Berlin, 1985.
- [30] K. Dechoum, P.D. Drummond, S. Chaturvedi, M.D. Reid, *Phys. Rev. A* 70 (2004) 053807.
- [31] M.K. Olsen, S.C.G. Granja, R.J. Horowicz, *Opt. Commun.* 165 (1999) 293.